ACS APPLIED MATERIALS & INTERFACES

Research Article

www.acsami.org

How to Optimize the Interface between Photosensitizers and TiO_2 Nanocrystals with Molecular Engineering to Enhance Performances of Dye-Sensitized Solar Cells?

Jiaxin Zheng,[†] Kai Zhang,[‡] Yanyan Fang,[§] Yunxing Zuo,[†] Yandong Duan,[†] Zengqing Zhuo,[†,∥] Xuanming Chen,[‡] Wanli Yang,[∥] Yuan Lin,[*,†,§] Man Shing Wong,[*,‡] and Feng Pan[*,†]

[†]School of Advanced Materials, Shenzhen Graduate School, Peking University, Shenzhen 518055, PR China

[‡]Department of Chemistry and Institute of Molecular Functional Materials, Hong Kong Baptist University, Kowloon Tong, Hong Kong SAR, PR China

[§]Beijing National Laboratory for Molecular Sciences, Key Laboratory of Photochemistry, Institute of Chemistry, Chinese Academy of Sciences, Beijing 100190, PR China

[∥]Advanced Light Source, Lawrence Berkeley National Laboratory, Berkeley, California 94720, United States

Supporting Information

ABSTRACT: In this work, the interfacial properties of a series of metal-free organic naphthodithienothiophene (**NDTT**)-based photosensitizers adsorbed on TiO_2 surfaces were investigated by a combination of ab initio calculations and experimental measurements. The calculations and experiments reveal that because of the efficient charge transfer from the adsorbed dyes to TiO_2 nanocrystal surface there is an upward shift for the energy levels of dyes and a downward shift for the conduction band of surface TiO_2 and that the band gaps for both of them are also reduced. Such electronic level alignments at the interface would lead to increased light absorption range by adsorbed dyes and increased driving force for charge injection but reduced open-circuit potential (V_{oc}). More interestingly, we found that molecule engineering of the donor group and introducing additional electron-withdrawing unit have little effect on the electronic level alignments at the interface (because band gaps of the dyes adsorbed on TiO_2 surfaces become approximately identical when compared with those of the dyes measured in solution) but that they can affect the steric effect and the charge separation at the interface to tune V_{oc} and the short-circuit current density (J_{sc}) effectively. All these findings suggest that optimizing the interfacial properties of dyes adsorbed on TiO_2 surfaces by synchronously modifying steric effects of dye molecules anchored on TiO_2 and charge-transfer and separation properties at the interfaces is important to construct efficient dye-sensitized solar cells.

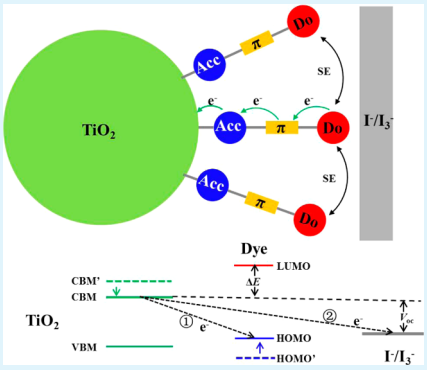

KEYWORDS: *DSSCs, metal-free photosensitizer, interface, steric effect, electronic structure, ab initio calculations*

INTRODUCTION

Dye-sensitized solar cells (DSSCs) have attracted considerable interest as an alternative renewable energy source in the decades since the seminal works by O'Regan and Grätzel.[1] Because of their intriguing advantages of low-cost fabrication, high molar extinction coefficient, and flexible tailor-making,[2] metal-free organic photosensitizers have recently drawn increasing attention in DSSC applications. Such organic photosensitizers generally possess a donor−π−acceptor (D−π−A) structure motif with strong intramolecular charge transfer (ICT) characteristics. To date, a record PCE of 13% has been reported by Grätzel and co-workers, using porphyrin−Zn(II)-based D−π−A photosensitizers.[3]

After absorption of light, charge separation is generally initiated at the interface between the dye bound to the TiO_2 surface and the hole-transporting material. The performance of DSSCs generally depends on not only the lowest unoccupied molecular orbital (LUMO), the highest occupied molecular orbital (HOMO), and their distributions of the photosensitizers but also the kinetics of the electron-transfer processes at the interface between the dye bound to the semiconductor surface and the hole-transporting material.[4] As a result, it is important that the microscopic interfacial properties of these all-organic metal-free dyes on TiO_2 photoanodes be investigated and understood including the anchoring state and charge transfer at the interface, band gap offset for the anchored dyes, HOMO and LUMO shift, and their redistributions. Meanwhile, the steric effect of the adsorbed dye molecules at the interface also plays an important role on the DSSC efficiency because the aggregation of the dye molecules on the TiO_2 surface may lead

Received: August 17, 2015
Accepted: October 28, 2015

DOI: 10.1021/acsami.5b07591
ACS Appl. Mater. Interfaces XXXX, XXX, XXX−XXX

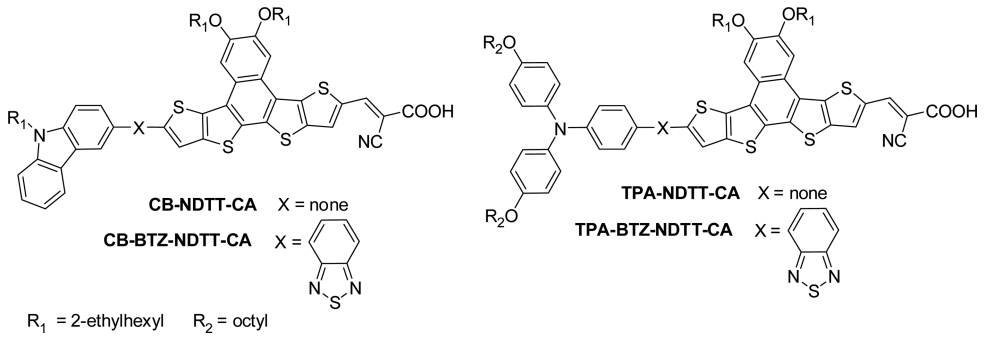

Figure 1. Molecular structures of **CB-NDTT-CA**, **TPA-NDTT-CA**, **CB-BTZ-NDTT-CA**, and **TPA-BTZ-NDTT-CA**.

to nonradiative decay of the excited state to the ground state, fast charge recombination, and low open-circuit voltage (V_{oc}).[5,6] In contrast, low dye-loading content on the TiO_2 surface would reduce the short-circuit current density (J_{sc}).

To construct an efficient all-organic dye for efficient DSSCs, lots of experimental studies have been focused on molecular engineering of photosensitizer molecules by modifying the structural component(s), including electron-donating groups, π-conjugated bridges, electron-accepting and anchoring groups, with which the optical, electronic, and photovoltaic properties can be fine-tuned. However, such modifications would also affect the interfacial properties between photosensitizers and TiO_2 surfaces,[6] and a detailed understanding of interfacial properties after molecular engineering is a prerequisite for the rational design of more robust and active sensitizers for photovoltaics.

Here we systematically studied the interfacial properties of a series of metal-free organic naphthodithienothiophene (**NDTT**)-based photosensitizers adsorbed on TiO_2 surfaces using ab initio calculations and experimental measurements. Calculations reveal that compared with the cyano groups of the dyes the binding of carboxylic groups on the TiO_2 surface is energetically favorable. The calculations and experiments also reveal that there is an upward shift for the energy levels of dyes and a downward shift for the conduction band of surface TiO_2 and that the band gaps for both of them are also reduced which is due to the efficient charge transfer from the adsorbed dyes to TiO_2 surface. Such electronic level alignments at the interface would lead to increased absorption range and increased driving force for charge injection but reduced open-circuit potential (V_{oc}). More interestingly, we found that molecular engineering of the donor group and introducing an additional electron-withdrawing unit have little effect on the electronic level alignments at the interface (because band gaps of the dyes become approximately identical when compared with those of the dyes measured in solution) but that they can affect the steric effect and the charge separation at the interface to tune V_{oc} and the short-circuit current density (J_{sc}) effectively.

METHODS

Computational Details. We carried out ab initio calculations applying density functional theory (DFT) as implemented in VASP code[7] and using projector-augmented wave methods with PW91 generalized gradient approximation (GGA) exchange correlation.[8] Because most available anatase TiO_2 crystals are dominated by the thermodynamically stable {101} facets (more than 94%, according to the Wulff construction),[9] considering only (101) surface of anatase TiO_2 is valid for experimental verification. This is also widely adopted in many other reported works.[10,11] We have applied the 4 × 5 × 4 anatase TiO_2 (101) supercell as the adsorption surface to prevent unfavorable aggregation of organic sensitizers on the surface. Because the exposed dangling bonds for each Ti and O atom of the surface can passivate each other, there is no need to consider the surface reconstruction to satisfy the electron-counting rule. A vacuum buffer space of at least 15 Å is set for slabs with adsorbed atoms, and dipole correction is employed to cancel artificial interactions between them. In our analysis of the functional groups of these four kinds of molecular dyes, **CB-NDTT-CA** and **CB-BTZ-NDTT-CA** are one type of molecule and **TPA-NDTT-CA** and **TPA-BTZ-NDTT-CA** are another type. We have investigated the behaviors of the organic dyes adsorbed on the TiO_2 surface and compare them with the behavior of molecules that were left intact. The protonation effect has also been taken into consideration. In contrast to another study focused on natural dyes on TiO_2 surface,[12] there is not much difference between the DOSs before and after the deprotonation.

Measurement of Absorption Spectra of Dye-Loaded TiO_2 films. A 1 layer film of TiO_2 nanoparticles was coated on a glass plate by the doctor-blade method. After sintering at 450 °C for 30 min, the TiO_2 film was immersed into the dye solutions in THF at room temperature for 5 h. Then, the UV−vis absorption spectrum of the dye-loaded TiO_2 film was recorded on a spectrophotometer (Model U-3010 UV Hitach).

Soft X-ray Spectroscopy. Soft X-ray absorption spectroscopy (XAS) is carried out at beamline 8.0.1 of the Advanced Light Source (ALS) at Lawrence Berkeley National Laboratory (LBNL). The undulator and spherical-grating monochromator supply a linearly polarized photon beam with resolving power up to 6000. The experimental energy resolution is better than 0.15 eV. All the XAS experiments are carried out at room temperature. All the spectra are collected in the both surface-sensitive total electron yield (TEY) and bulk-sensitive total fluorescence (TFY) modes. The probing depth of TEY is around 10 nm, and that of TFY is around 150 nm. All the spectra are normalized to the photon flux measured by the photocurrent of an upstream gold mesh.

RESULTS AND DISCUSSION

Experimental System. Because of their rigid, planar, and high charge-carrier mobility nature, naphtho[2,1-*b*:3,4-*b*′]-dithiophene and its derivatives have been extensively used as a π-conjugated building block to develop efficient organic semiconducting materials for organic photovolatics and thin-film transistors.[13,14] A more π-extended electron-rich analog, naphtho[1,2-*b*:4,3-*b*′]dithieno[3,2-*b*]thiophene (**NDTT**)[15] is anticipated to be more beneficial to enhance the π-electron delocalization, broad and longer wavelength absorption, and efficient charge transfer, thus giving rise to a higher light harvest efficiency and increased electron injection.[16] Besides the D−π−A structure motif, an alternative structural architecture, namely, D−A−π−A, has been adopted recently in which an auxiliary accepting unit such as benzothiadiazole (**BTA**) is incorporated between the electron-donating moiety and the π-conjugated bridge in order to enhance the intramolecular charge transfer,

DOI: 10.1021/acsami.5b07591
ACS Appl. Mater. Interfaces XXXX, XXX, XXX−XXX

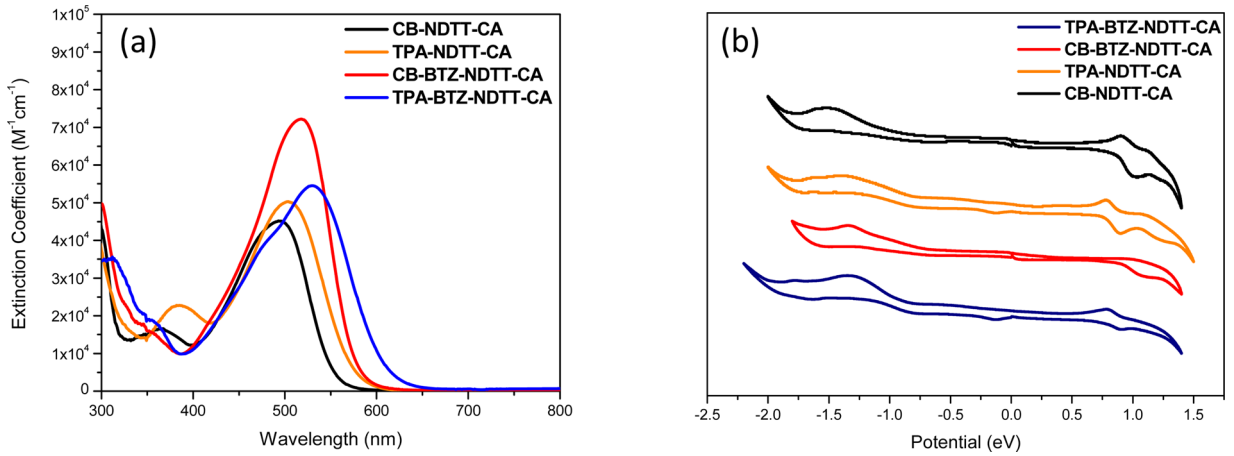

Figure 2. (a) Absorption spectra of **CB-NDTT-CA**, **TPA-NDTT-CA**, **CB-BTZ-NDTT-CA**, and **TPA-BTZ-NDTT-CA** in THF. (b) CV traces of **CB-NDTT-CA**, **TPA-NDTT-CA**, **CB-BTZ-NDTT-CA**, and **TPA-BTZ-NDTT-CA**.

Table 1. Results of Optical and Electrochemical Measurements of CB-NDTT-CA, TPA-NDTT-CA, CB-BTZ-NDTT-CA, and TPA-BTZ-NDTT-CA

compound	λ_{max}^{abs} (ε)[a]	optical gap (eV)[a,b]	E_p^{oxd} (eV)[c]	E_p^{red} (eV)[c]	HOMO (eV)[d]	LUMO (eV)[d]	EG[e]
CB-NDTT-CA	486 (4.93)	2.24	0.87	−0.89	−5.11	−3.35	1.76
TPA-NDTT-CA	498 (5.50)	2.15	0.76	−0.87	−5.00	−3.37	1.63
CB-BTZ-NDTT-CA	513 (6.46)	2.13	0.89	−0.70	−5.13	−3.52	1.61
TPA-BTZ-NDTT-CA	531 (6.95)	2.02	0.77	−0.78	−5.01	−3.46	1.55

[a] λ_{max}^{abs} given in nanometers. Measured in THF ($\varepsilon \times 10^4$ M^{-1} cm^{-1}). [b] Estimated from the absorption edge in THF; optical band gap =1240/λ_{onset}^{abs} eV. [c] Determined by the CV method using a platinum disc electrode as the working electrode, platinum wire as the counter electrode, and SCE as the reference electrode with an agar salt bridge connecting to the solution of oligomers in THF. Ferrocene was used as the external standard, $E_{1/2}$ (Fc/Fc^+) = 0.56 eV vs SCE. [d] Calculated from the first oxidation potential with ferrocene (4.8 eV vs vacuum). [e] EG = LUMO − HOMO.

light harvesting, and photostability of the resulting photosensitizer molecule.[17−19]

The molecular structures of novel naphthodithienylthiophene-based photosensitizers are shown in Figure 1, and their synthesis are outlined in Schemes S1 and S2. The starting substrates **1**−**4** are synthesized according to procedures reported previously.[15,20−22] Triarylamine or carbazole was used as an electron-donating group, benzothiadiazole acted as an auxiliary electron-accepting unit, and cyanoacrylic acid played the role of an electron-accepting and anchoring group. In addition, to improve the solubility and reduce the $\pi-\pi$ aggregation of photosensitizer molecules on the TiO_2 surface that could decrease charge recombination and thus enhance the open circuit voltage (V_{oc}),[23] the branched alkoxyl chains were incorporated onto the naphthalenedithienylthiophene moiety.

For the carbazole-donor series, the palladium-catalyzed Suzuki coupling of carbazole-based boronate ester **1** with 1,4-dibromobenzothiadiazole afforded the intermediate **5** in an excellent yield, followed by the Miyaura borylation with bis(pinacolato)diboron catalyzed by $Pd(dppf)_2Cl_2$ using KOAc as a base, affording carbazole-substituted benzothiadiazoleboronate ester **6**. In contrast, double Suzuki cross-coupling of dibromobenzene derivative **2** with boronate ester **3** gave bisthienylthiophene intermediate **7** in good yield, followed by $FeCl_3$-catalyzed ring-closure reaction, yielding naphthodithienylthiophene **8**. Monobromination of **8** by means of NBS in THF yielded bromonaphthodithienylthiophene **9**. Subsequent Vilsmeier−Haack reaction of **9** gave bromonaphthodithienylthiophenealdehyde **10** in good yield. The palladium-catalyzed Suzuki cross coupling of **10** with the corresponding donor boronate esters, **1** or **6**, yielded the carbazole-substituted naphthodithienylthiophene intermediate, **11** or **12**, respectively. The condensation reaction of aldehyde **11** or **12** with 2-cyanoacetic acid catalyzed by NH_4OAc in AcOH afforded the desired **CB-NDTT-CA** and **CB-BTZ-NDTT-CA**, respectively, in good yield.

For the triarylamino-donor series, diarylaminophenylboronate ester **13** was prepared by Miyaura borylation of bromide **4** with bis(pinacolato)diboron. The palladium-catalyzed Suzuki coupling of **13** with 1,4-dibromobenzothiadiazole yielded the intermediate **14**, followed by a facile Miyaura borylation affording triarylamino-substituted benzothiadiazoleboronate ester **15**. Then, the palladium-catalyzed Suzuki coupling of bromo-naphthodithienylthiophenealdehyde **10** with the corresponding boronate ester, **13** or **15**, gave the coupled aldehyde, **16** or **17**, respectively, in good yield. Condensation of aldehyde **16** or **17** with 2-cyanoacetic acid afforded the desired dye **TPA-NDTT-CA** or **TPA-BTZ-NDTT-CA**, respectively, in excellent yield.

The thermal properties of the newly synthesized naphthodithienylthiophene-based photosensitizers were first examined by thermogravimetric analysis (TGA). All these photosensitizers exhibit good thermal stability with decomposition temperatures above 250 °C under inert atmosphere (Figure S1).

Energy Levels of the Dyes in THF Solution. The absorption spectra of **CB-NDTT-CA**, **CB-BTZ-NDTT-CA**, **TPA-NDTT-CA**, and **TPA-BTZ-NDTT-CA** measured in THF solution are shown in Figure 2a. These photosensitizing dyes exhibit distinct strong and broad absorptions peaked at 475−550 nm, corresponding to intramolecular charge-transfer transition, and a moderate absorption around 300 nm,

DOI: 10.1021/acsami.5b07591
ACS Appl. Mater. Interfaces XXXX, XXX, XXX−XXX

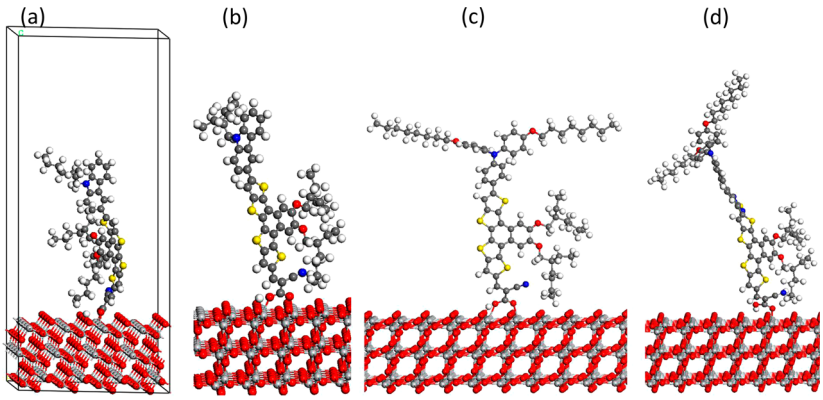

	CB-NDTT-CA	TPA-NDTT-CA	TPA-BTZ-NDTT-CA
E_{ads} (eV)	2.4	2.5	1.5
d_{Ti-O} (Å)	2.0	2.1	2.01

Figure 3. Ab initio calculations for the dye molecules/TiO_2 interfaces. (a) Unit cell with **CB-NDTT-CA** molecule adsorbed on TiO_2 anatase (101) surface. (b–d) Most energy stable adsorption structures of **CB-NDTT-CA** (b), **TPA-NDTT-CA** (c), and **TPA-BTZ-NDTT-CA** (d) on TiO_2 (101) surface. The table shows adsorption energies (E_{ads}) and geometry parameters for all adsorption configurations on TiO_2.

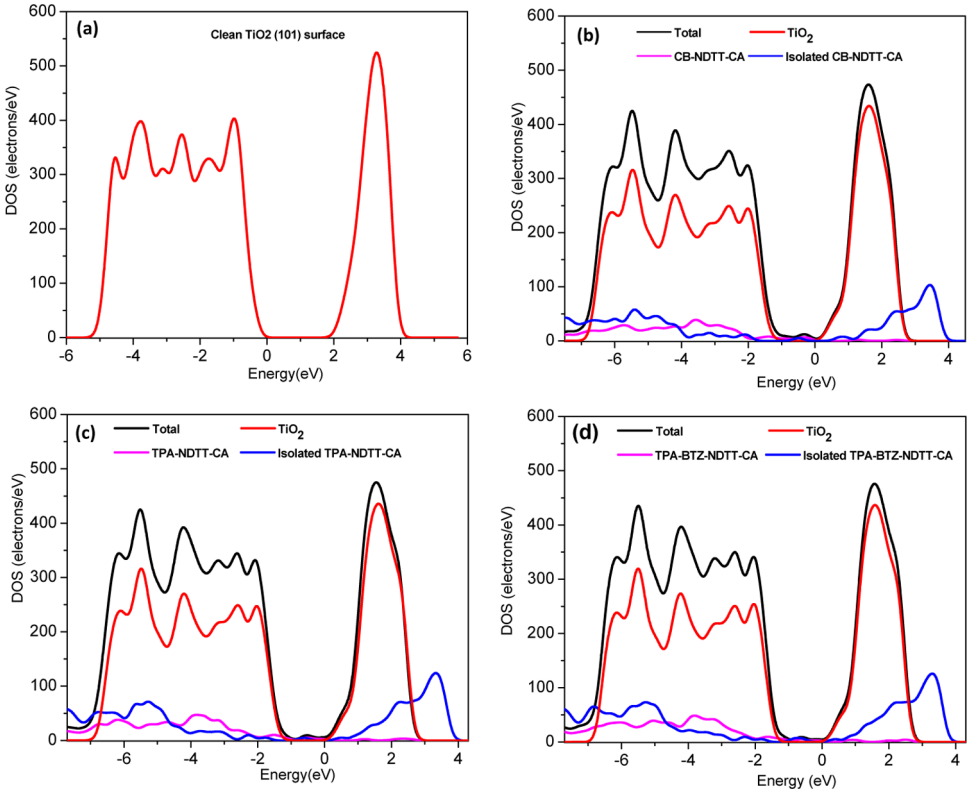

Figure 4. Calculated total density of states (DOS) and projected density of states (PDOS) for (a) clean TiO_2 surface and interfaces of TiO_2 adsorbed with **CB-NDTT-CA** (b), **TPA-NDTT-CA** (c), and **TPA-BTZ-NDTT-CA** (d).

corresponding to n–π^* transition, which are typical absorption characteristics of donor–acceptor-type π-conjugated molecules. There is a significant bathochromic shift of the absorption maximum concomitant with an increase in molar absorptivity upon an incorporation of electron-deficient benzothiadiazole (**BTA**) unit into the π-conjugated backbone. This is attributed to the increased conjugation length and enhanced intermolecular charge transfer along the π-conjugated backbone. In addition, the strong donating triarylamine group induces a larger bathochromic shift of the absorption spectrum relative to those of carbazole-based counterparts. The optical band gaps of these photosensitizers deduced from the onset of their absorption spectra measured in THF solution are in the range of 2.02–2.24 eV (Table 1), which are also consistent with

DOI: 10.1021/acsami.5b07591
ACS Appl. Mater. Interfaces XXXX, XXX, XXX–XXX

the results of the excitation spectra and the room-temperature photoluminescence (PL) spectra (Figure S2).

The electrochemical characteristics of these photosensitizers were determined by cyclic voltammetry (CV) in THF using a platinum disc electrode as the working electrode, platinum wire as the counter electrode, and saturated calomel electrode (SCE) as the reference electrode in 0.1 M of Bu_4NPF_6 with a scan rate of 100 mV/s. The resulting CV traces are shown in Figure 2b. The energy levels of HOMO and LUMO were estimated from the onset of the oxidation and reduction waves, respectively (Table 1). The HOMO energy levels of **CB-NDTT-CA** and **TPA-NDTT-CA** were estimated to be −5.11 and −5.00 eV, respectively. Because of an incorporation of electron-deficient **BTA** unit, the HOMO energy levels of **CB-BTZ-NDTT-CA** and **TPA-BTZ-NDTT-CA** are slightly stabilized and lowered to −5.13 and −5.01 eV, respectively. However, the band gaps of these photosensitizers estimated from the onset of the oxidation and reduction waves are in the range of 1.55−1.76 eV, which is smaller than the optical band gaps measured in THF solution by ∼0.5 eV. The smaller band gaps measured by CV method compared with the optical band gaps measured in THF solution are most probably attributed to the charge transfer between the dye molecules and the electrode surfaces, as indicated in the following ab initio calculations.

Geometry and Stability of Dyes on TiO_2 Surfaces. To get an in-depth picture of the NDTT based dye/TiO_2 interface, we carried out ab initio calculations to study the adsorption structures of three representative kinds of **NDTT**-type dyes (**CB-NDTT-CA**, **TPA-NDTT-CA**, and **TPA-BTZ-NDTT-CA**) on TiO_2. Figure 3a shows a representative supercell model for **CB-NDTT-CA** adsorption. A 9 layer (4 × 4) TiO_2 slab (total 144 atoms) is used to model the anatase (101) surface, and the bottom six layers are fixed to simulate the bulk geometry. This model gives a reliable description of surface electronic structure, and the calculated lattice constants of $a = b = 3.82$ Å and $c = 9.66$ Å also agree well with experimental values of 3.79 and 9.51 Å.[24] We have estimated the stability of different adsorption model from total energy calculation, discovering that the bridging model is the most stable binding form and is more stable than the esterlike model in contrast to previous studies on other organic dye adsorbed on TiO_2 surface.[25,26] Figure 3b−d shows the most energy stable adsorption structures for all-**NDTT**-type dyes on anatase (101). All structures except Figure 3d show a bidentate adsorption conformer with two interface Ti−O bonds via the carboxylic groups, and the binding energies for **CB-NDTT-CA**, **TPA-NDTT-CA**, and **TPA-BTZ-NDTT-CA** are 2.4, 2.5, and 1.5 eV, respectively. This bidentate configuration was also always thought to be the most stable in previous works,[27] and the strong chemical bonding maintains the interface stability of **NDTT**-type dyes solar cells.

Ab Initio Calculated Electronic Structures of the Dyes/TiO_2 Interfaces. We next examined the electronic structures for clean and dye-adsorbed anatase (101) surfaces. Figure 4 shows the density of states (DOS) and projected density of states (PDOS) for all the adsorption configurations. Compared with the clean (101) surface, the conduction band of surface TiO_2 is shifted downward, and the band gaps of surface TiO_2 for all samples are reduced after the dye adsorption (from 1.8 eV for clean surface to around 1.25 eV after dye adsorption). This can be attributed to the charge transfer between the TiO_2 and dye molecules, which would build a favorable dipolar field at the interface to tune the band energy levels of the surface TiO_2.[27] This band gap reduction for the TiO_2 surface would facilitate the electron transport and increase the gap between the LUMO of dyes and CBM of TiO_2, thus increasing the driving force for charge injection at the interface. However, the downward shift of the conduction band of the surface TiO_2 would also lead to reduced V_{oc}. Furthermore, we can see that the DOS of dye molecules shift to higher energy after adsorption (compared with isolated dye molecules), indicating a significant charge (electron) transfer from dye molecules to TiO_2 surface. The HOMOs of molecules have shifted into the band gap region of TiO_2, and LUMOs moved 0.5−0.9 eV higher than the conduction band minimum (CBM) of the TiO_2 surface, providing sufficient driving force for charge injection, which is critical for solar cell applications.

The band gaps (the energy gap between the HOMO and LUMO) of isolated **CB-NDTT-CA**, **TPA-NDTT-CA**, and **TPA-BTZ-NDTT-CA** dye molecules are 1.50, 1.15, and 0.98 eV, with LUMO changing only slightly around −3 eV (Table 2). Interestingly, band gaps are narrowed into 0.97, 0.87, and 0.91 eV after being adsorbed on TiO_2 surface for **CB-NDTT-CA**, **TPA-NDTT-CA**, and **TPA-BTZ-NDTT-CA** molecules (Table 2), indicating that the absorption range for the dyes is increased and that the band gap differences for these molecules are reduced. Thus, these results suggest that molecular engineering of the donor group or introducing an additional electron-withdrawing unit (**BTZ**) has little effect on the electronic level alignments at the interface with the dyes loading on TiO_2 surfaces. The Bader charge analysis[28,29] of the VASP results reveals the similar charge transfer from the dye molecules to TiO_2 surface (Table 2), which can be attributed to the same electron-accepting and anchoring group of **CA** for all dye molecules.

Table 2. Ab Initio (VASP) Calculated Band Gaps Before (E_{g1}) and After Adsorption (E_{g2}) for Dye Molecules[a]

	CB-NDTT-CA	TPA-NDTT-CA	TPA-BTZ-NDTT-CA
E_{g1} (eV)	1.50	1.15	0.98
E_{g2} (eV)	0.97	0.87	0.91
Q	0.24	0.30	0.25

[a]Q denotes the electrons transferred from dye molecules to TiO_2 surfaces.

To clarify the mechanisms behind the above phenomenon, we additionally calculated the molecular orbitals of the three kinds of dyes using the Gaussian09 package[30] for comparison. A BLYP functional was adopted, and the 6-31G* is set as Gaussian basis with polarization functions.[31,32] We also calculated the molecular orbitals of the three kinds of dyes with one added positive charge, which simulates the case of electrons being transferred from dye molecules to TiO_2 surface. Figures 5 and 6 presented the calculated HOMOs and LUMOs for the three kinds of dye molecules. Though the band gaps calculated from Gaussian09 (Table 3) are close to the optical band gaps of these photosensitizers deduced from the onset of their absorption spectra measured in THF solution and are larger than those calculated from VASP package (based on the plane wave basis) by nearly 60%, both methods show the same trend that the band gap differences for these molecules are reduced when the electrons are transferred out or positive charge is added. In these three dye molecules, the LUMOs are largely populated along the acceptor groups and π bridge, and

DOI: 10.1021/acsami.5b07591
ACS Appl. Mater. Interfaces XXXX, XXX, XXX−XXX

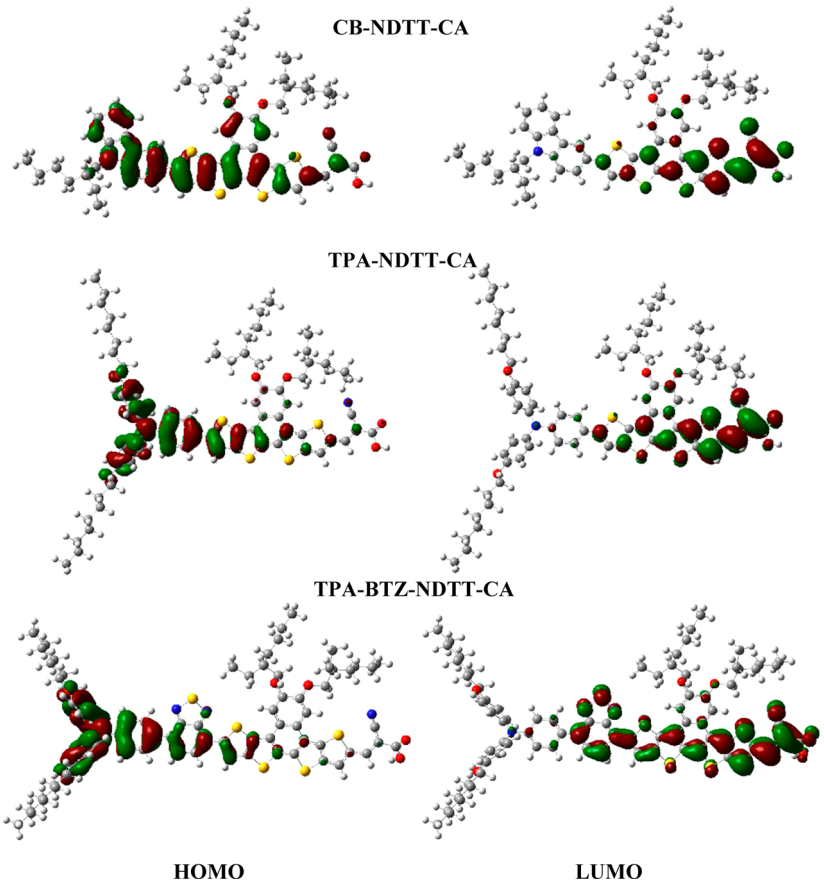

Figure 5. Frontier orbitals of **CB-NDTT-CA**, **TPA-NDTT-CA**, and **TPA-BTZ-NDTT-CA**.

the HOMOs are mainly localized in donor units for **TPA-NDTT-CA** and **TPA-BTZ-NDTT-CA** but spread to π bridge for **CB-NDTT-CA**, providing evidence for weak intramolecular charge transfer for **CB-NDTT-CA** and leading to the largest band gap. However, when adsorbed on the TiO_2 surface, both HOMOs and LUMOs become delocalized for all these dye molecules, and the capability of intramolecular charge transfer becomes identical, thus leading to the narrowed band gaps and little band gap differences for these molecules.

Confirmation by Experiment: Soft X-ray Emission and Absorption Spectroscopy and UV−Vis Absorption Measurements. Soft X-ray emission spectroscopy (XES) and soft X-ray absorption spectroscopy (XAS) are used to detect the electronic structure variation of the TiO_2 surface with and without dye loading (Figure 7). It can be observed that the valence band remains nearly unchanged and the conduction band shifts downward after dye absorption (Figure 7, clearly for **CB-TPA-NDTT-CA** and **TPA-BTZ-NDTT-CA** absorption) which confirmed our ab initio calculations. Next, we recorded the UV−vis diffuse reflectance spectra of the dyes anchored on TiO_2 films at different dye concentrations after 5 h adsorption (Figure 8). It was found that there was minor difference among different concentrations suggesting that aggregation of dye molecules on the surface of TiO_2 films was negligible. More interestingly, compared with the optical band gaps of these photosensitizers measured in THF solution, the band gaps of these photosensitizers absorbed on TiO_2 films have become smaller and approximately identical, estimated to be 1.80−1.78 eV (around 686 nm ~695 nm) from the onset of the diffuse reflectance spectra (Figure 8), which is very consistent with the ab initio calculation predictions.

Photovoltaic Parameters and Recombination. Finally, we fabricated DSSCs using these **NDTT**-based photosensitizers and investigated their photovoltaic properties. The typical current−voltage (I−V) characteristics at AM 1.5 simulated sunlight are shown in Figure 9 with the corresponding performance parameters summarized in Table S1. The solar cell based on **CB-NDTT-CA** shows an efficiency of 7.29%, with a short-circuit photocurrent density (J_{sc}) of 14.48 mA cm^{-2}, an open-circuit photovoltage (V_{oc}) of 695 mV, and a fill factor (FF) of 0.724. The solar cell based on **TPA-NDTT-CA** only shows an efficiency of 5.33%, with a J_{sc} of 11.0 mA cm^{-2}, a V_{oc} of 718 mV, and a FF of 0.675. The lower efficiency of **TPA-NDTT-CA** based device can be attributed to the decreased J_{sc} and FF after replacing carbazole-donor with triarylamino donor. Because of the large and bulky triarylamino donor, the dye-loading content of **TPA-NDTT-CA** on TiO_2 is less than that of carbazole-donor analog, **CB-NDTT-CA**, which accounts for the reduced J_{sc}. The lower dye-loading content of **TPA-NDTT-CA** is reflected by the absorption spectra of TiO_2 films sensitized with one layer of dye molecules (Figure S4). The thickness of the adsorbed dyes is kept to 3 um for all the samples. We can see that the absorption degree of **TPA-NDTT-CA** is weaker than that of **CB-NDTT-CA**, indicating a lower dye-loading content on TiO_2 films for **TPA-NDTT-CA**. In contrast, this large and bulky triarylamino donor can limit aggregation between the dye molecules, which is a recurrent problem during device fabrication and operation, and prevents the charge recombination between the TiO_2 surface and I^-/I_3^- in

DOI: 10.1021/acsami.5b07591
ACS Appl. Mater. Interfaces XXXX, XXX, XXX−XXX

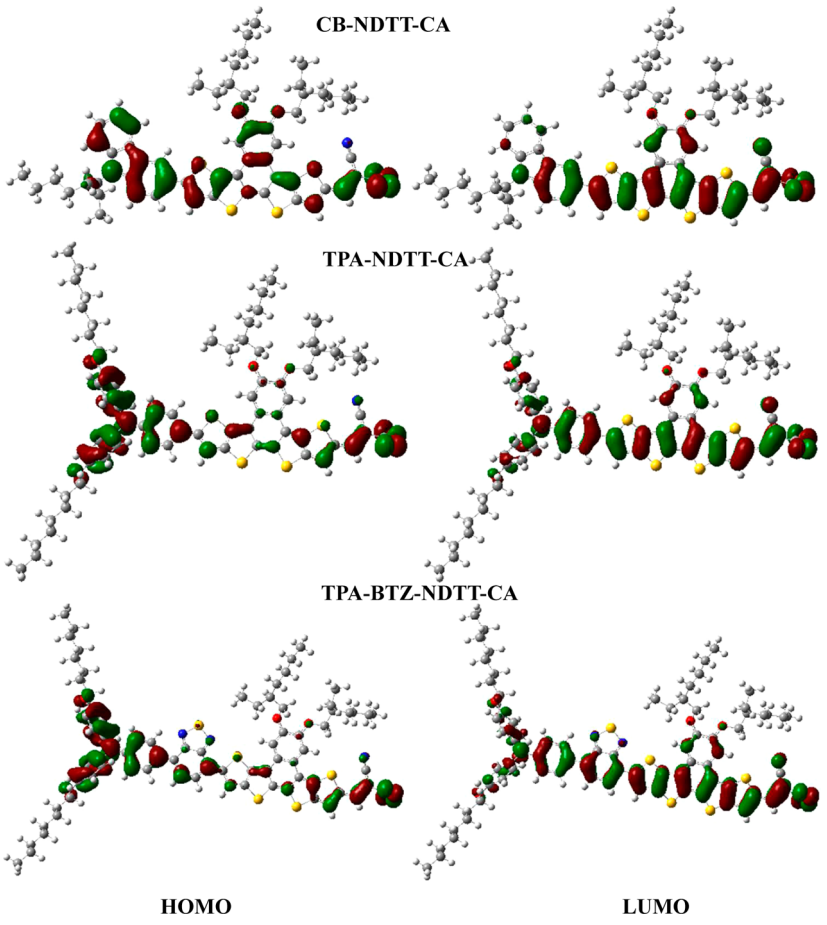

Figure 6. Frontier orbitals of **CB-NDTT-CA**, **TPA-NDTT-CA**, and **TPA-BTZ-NDTT-CA** with one added positive charge.

Table 3. Calculated Band Gaps for Neutral (E_{g1}) and Positively Charged (E_{g2}) Dye Molecules by Gaussian09 Package

	CB-NDTT-CA	TPA-NDTT-CA	TPA-BTZ-NDTT-CA
E_{g1} (eV)	2.38	2.02	1.84
E_{g2} (eV)	0.92	0.96	1.01
reduction (eV)	1.46	1.06	0.83

the electrolyte. Moreover, the strong electron-rich triarylamino donor also induces a HOMO more localized on the donor part (Figure 5) to suppress the charge recombination between TiO_2 and dyes.[4] All the above reasons lead to the increased V_{oc}. This is further confirmed by the Nyquist plots of electrochemical impedance spectroscopy (EIS) and intensity-modulated photovoltage spectroscopy (IMVS) measurements of the DSSCs (Figure S5, S6 and Table S2). The larger semicircles in lower-frequency in EIS reflect the recombination resistance (R_{ct2}) at TiO_2/electrolyte interface. The radius of the semicircle for **TPA-NDTT-CA** is larger than that of **CB-NDTT-CA**, indicating a smaller charge recombination rate for **TPA-NDTT-CA** and consistent with its increased V_{oc}. The electron

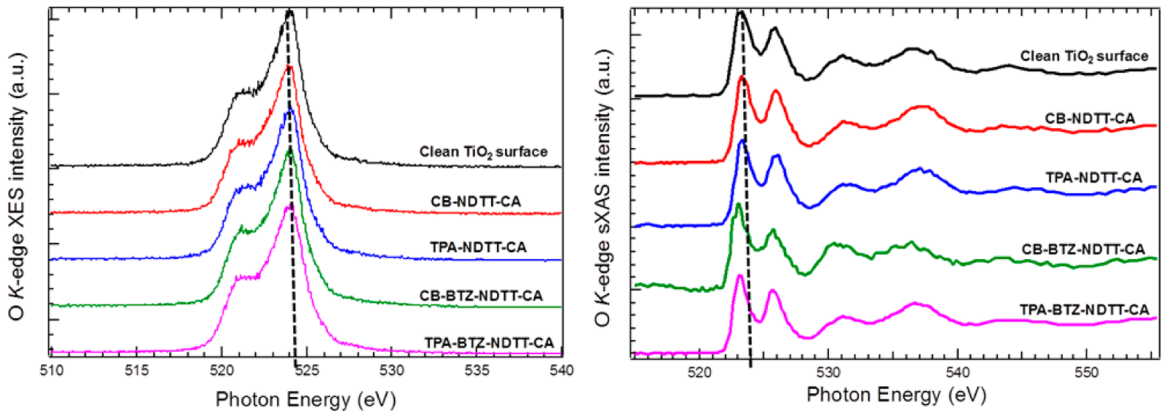

Figure 7. Soft X-ray emission spectroscopy (XES) (left) and soft X-ray absorption spectroscopy (XAS) (right) of clean TiO_2 surfaces and TiO_2 surfaces adsorbed with **CB-NDTT-CA**, **TPA-NDTT-CA**, **CB-BTZ-NDTT-CA**, and **TPA-BTZ-NDTT-CA**.

DOI: 10.1021/acsami.5b07591
ACS Appl. Mater. Interfaces XXXX, XXX, XXX−XXX

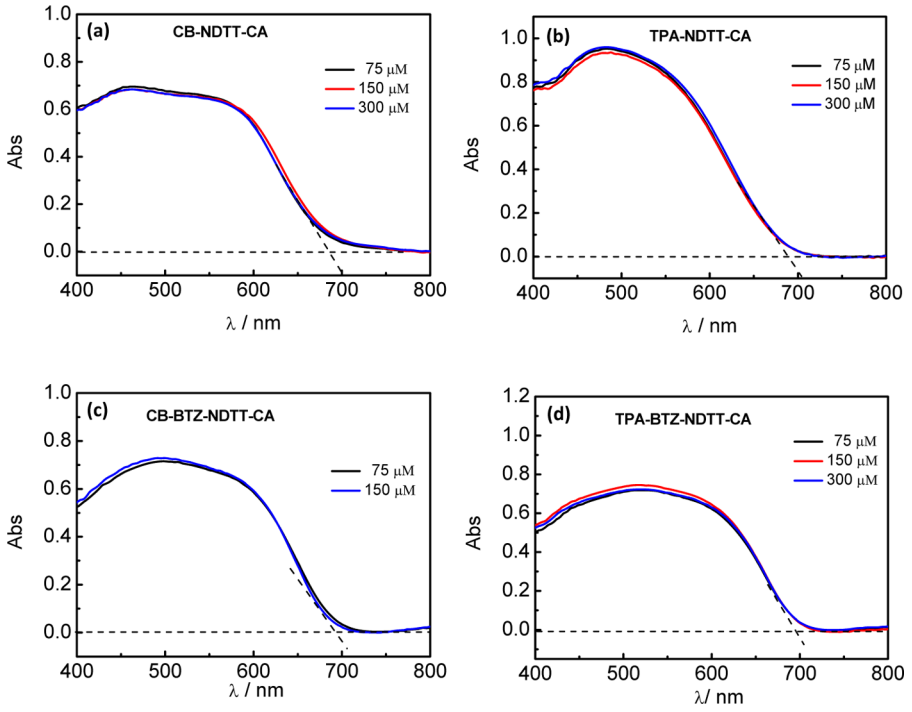

Figure 8. UV−vis diffuse reflectance spectra for TiO_2 films sensitized with different concentration of **CB-NDTT-CA** (a), **TPA-NDTT-CA** (b), **CB-BTZ-NDTT-CA** (c), and **TPA-BTZ-NDTT-CA** (d).

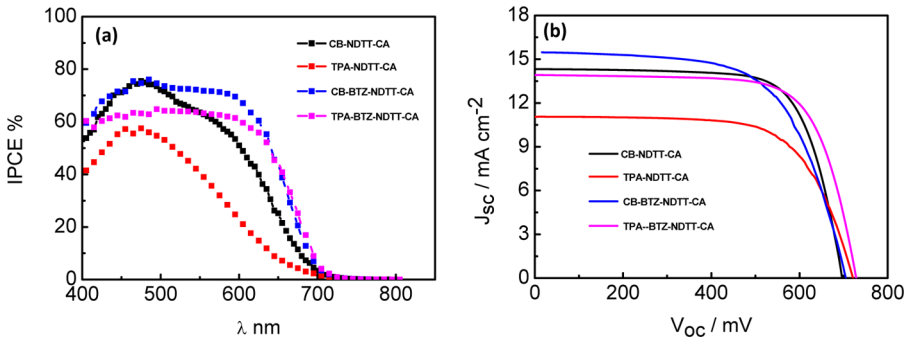

Figure 9. IPCE spectra (a) and *J*−*V* curves (b) of DSSCs with **CB-NDTT-CA**, **TPA-NDTT-CA**, **CB-BTZ-NDTT-CA**, and **TPA-BTZ-NDTT-CA**.

lifetime (τ_n) can be estimated by the equation $\tau = (2\pi f_{min})^{-1}$, where f_{min} is the frequency of the minimum of the IMVS imaginary component. The electron lifetime of **TPA-NDTT-CA** (159.2 ms) is larger than that of **CB-NDTT-CA** (126.5 ms), also indicating a suppressed charge recombination for **TPA-NDTT-CA**.

Once a **BTZ** unit is introduced as an additional electron-withdrawing unit into the π bridge of **CB-NDTT-CA**, affording **CB-BTZ-NDTT-CA**, the improved J_{sc} (15.47 mA cm^{-2}) and V_{oc} (700 mV) are observed. Such enhancement in device performance is also observed when a **BTZ** unit is introduced into **TPA-NDTT-CA** to construct **TPA-BTZ-NDTT-CA** (J_{sc}= 13.91 mA cm^{-2}; V_{oc} = 725 mV). The density functional theory (DFT) simulation indicates that the distributions of both HOMO and LUMO orbitals for sensitizers **TPA-BTZ-NDTT-CA** are overlapped with those of the **BTZ** unit (Figure 5), indicating the preferably facilitated electron transfer from HOMO to LUMO orbitals. Convincingly, the cascaded electron withdrawal from donor (D) to internal acceptor (A), then to terminal A in the D−A−π−A configuration may benefit charge separation in organic sensitizers, thus leading to the increased J_{sc} and V_{oc}. This is also confirmed by the IMVS measurements (Figure S6 and Table S2), which show that the electron lifetime of **TPA-BTZ-NDTT-CA** (503.9 ms) is larger than that of **TPA-NDTT-CA** (224.9 ms) indicating that the **BTZ** unit introduced into the π bridge can enhance the charge separation in organic sensitizers. As a result, compared with **TPA-NDTT-CA**, the efficiency of **TPA-BTZ-NDTT-CA** is improved from 5.33 to 7.22%. In contrast, despite the improved J_{sc} and V_{oc}, the final efficiency of **CB-BTZ-NDTT-CA** is decreased from 7.29 to 6.85% compared with that of **CB-NDTT-CA**, which is mainly due to the greatly decreased FF from 0.724 for **CB-NDTT-CA** to 0.632 for **CB-BTZ-NDTT-CA**. This is mainly attributed to the large J_{sc} for the sample of **CB-BTZ-NDTT-CA**, which would reduce FF and is also usually observed in other DSSCs.[33−35] The above photovoltaic properties demonstrated that though molecular engineering of the donor group and introduction of an additional electron-withdrawing unit (**BTZ**) have little effect on the electronic level alignments and the absorption range for the dyes at the interface with dyes loading on TiO_2 surfaces they still affect the

DOI: 10.1021/acsami.5b07591
ACS Appl. Mater. Interfaces XXXX, XXX, XXX−XXX

steric effect and the charge separation at the interface effectively.

All the theoretical and experimental findings in this work can be summarized in Figure 10, which proposes how to optimize

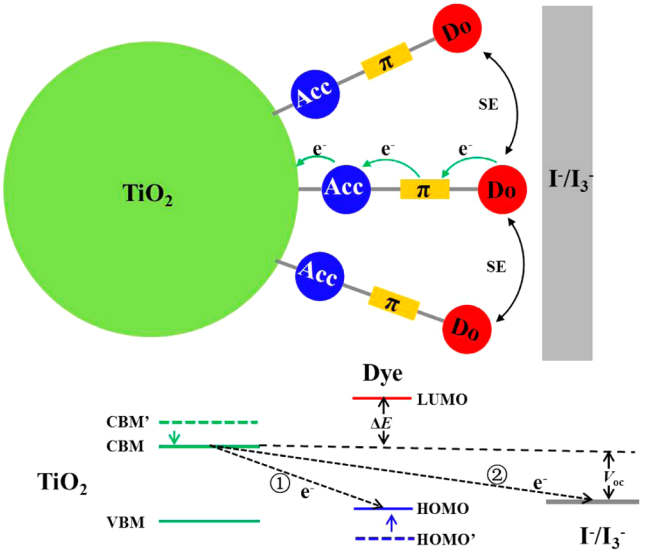

Figure 10. Schematic model of the dye/TiO_2 interface and energy-level diagram of a DSSC. SE denotes the steric effect among the dye molecules adsorbed on the TiO_2 surfaces. ΔE is defined as the difference between the energy level of the dye's LUMO and the CBM of the TiO_2. CBM′ denotes the original valence band maximum of surface TiO_2 before dye adsorption, and HOMO′ denotes the original HOMO level of dye molecules before adsorption on TiO_2. Process 1 (①) denotes the charge recombination between electrons at TiO_2 surface and holes of the dyes; process 2 (②) denotes the charge recombination between electrons at TiO_2 surface and the redox mediator (I^-/I^-_3).

the interface between photosensitizers and TiO_2 nanocrystals with molecular engineering to enhance performances of dye-sensitized solar cells. When the dyes are anchored on TiO_2 films, there is an efficient charge transfer from the dyes to TiO_2, thus leading to the energy level alignment at the interface: an upward shift for the energy levels of dyes (only showing the shift of HOMO relative to LUMO) and a downward shift for the conduction band of surface TiO_2, accompanied by reduced band gaps for both of them. The downward shift of CBM means an increased driving force for charge injection with the disadvantage of reduced V_{oc}, and the reduced band gap for dyes means increased absorption range. Compared with the band gaps obtained in THF solution, the band gaps of photosensitizers absorbed on TiO_2 films become approximately identical, which is found and systemically studied for the first time, indicating that molecular engineering of the donor group and introduction of an additional electron-withdrawing unit (**BTZ**) have little effect on the electronic level alignments and the absorption range for the dyes at the dye/TiO_2 interface. The more efficient way to tune the electronic level alignments at the interface is molecular engineering of the anchoring group of dyes, e.g., cyano group anchoring could induce different electronic level alignments at the interface from carboxylic/carboxylate groups.[10] However, molecular engineering of the donor group and introduction of an additional electron-withdrawing unit can affect the steric effect and the charge separation at the interface to tune J_{sc} and V_{oc} effectively. The steric effect at the interface could tune the dye-loading content and the charge recombination between the TiO_2 and redox mediator in the electrolyte (Figure 10, process 2). Molecular engineering of the donor group and introduction of an additional electron-withdrawing unit can also make the positive charge resulting after electron injection be more localized on the donor part and enhance the charge separation in dyes to minimize charge recombination between the injected electrons and the resulting oxidized dye (Figure 10, process 1).

CONCLUSIONS

Using ab initio calculations and experimental measurements, we systematically studied the interfacial properties of a series of metal-free organic **NDTT**-based photosensitizers adsorbed on TiO_2 surfaces. We first found that because of the efficient charge transfer from the dyes to the TiO_2 there is an upward shift for the energy levels of dyes and a downward shift for the conduction band of surface TiO_2 and that the band gaps for both of them are also reduced. We next found that molecular engineering of the donor group and introduction of an additional electron-withdrawing unit have little effect on the electronic level alignments and the absorption range for the dyes at the dye/TiO_2 interface because band gaps of the dyes adsorbed on TiO_2 surfaces become approximately identical when compared with those of the dyes measured in solution. However, they can affect the steric effect and the charge separation at the interface effectively. Hence, the interfacial properties of dyes adsorbed on TiO_2 surfaces with molecular engineering can be optimized for high-performance DSSC by synchronously modifying steric effects of dye molecules anchored on specifically orientated surfaces of nanocrystals and charge-transfer properties in a dye and at the interface between dyes and nanocrystals. We believe that such a fundamental understanding of the photosensitizers/TiO_2 interface would share microscopic mechanisms for further dye design and interface optimization for practical DSSC applications.

ASSOCIATED CONTENT

Supporting Information

The Supporting Information is available free of charge on the ACS Publications website at DOI: 10.1021/acsami.5b07591.

Details about materials and methods; schemes of synthesis of **CB-NDTT-CA**, **CB-BTZ-NDTT-CA**, **TPA-NDTT-CA**, and **TPA-BTZ-NDTT-CA**; their TGA traces; their room temperature photoluminescence (PL) excitation and emission spectra in THF; IPCE spectra of DSSCs; J-V curves for DSSCs; detailed photovoltaic parameters of DSSCs with four dyes; absorption spectra of TiO_2 films sensitized with one layer of **CB-NDTT-CA**, **TPA-NDTT-CA**, **CB-BTZ-NDTT-CA**, and **TPA-BTZ-NDTT-CA**; Nyquist plots from impedance spectra, IMVS and IMPS spectra of the DSSCs based on four dyes. (PDF)

AUTHOR INFORMATION

Corresponding Authors

*E-mail: linyuan@iccas.ac.cn.
*E-mail: mswong@hkbu.edu.hk.
*E-mail: panfeng@pkusz.edu.cn.

Author Contributions

J.Z., K.Z., and Y.F. contributed equally to this work.

DOI: 10.1021/acsami.5b07591
ACS Appl. Mater. Interfaces XXXX, XXX, XXX−XXX

Notes

The authors declare no competing financial interest.

■ ACKNOWLEDGMENTS

The research was financially supported by Guangdong Innovation Team Project (no. 2013N080), Shenzhen peacock plan (grant no. KYPT20141016105435850), Shenzhen Science and Technology Research Grant (nos. ZDSY20130331145131323, CXZZ20120829172325895, and JCYJ20120614150338154). This work was also supported by GRF (HKBU 203212), Hong Kong Research Grant Council and Institute of Molecular Functional Materials, which was supported by a grant from the University Grants Committee, Areas of Excellence Scheme (AoE/P-03/08).

■ REFERENCES

(1) O'Regan, B.; Gratzel, M. A Low-Cost High-Efficiency Solar Cell Based on Dye-Sensitized Colloidal TiO_2 Films. *Nature* **1991**, *353*, 737−740.

(2) Caballero, R.; Barea, E. M.; Fabregat-Santiago, F.; de la Cruz, P.; Márquez, L.; Langa, F.; Bisquert, J. Injection and Recombination in Dye-Sensitized Solar Cells with a Broadband Absorbance Metal-Free Sensitizer Based on Oligothienylvinylene. *J. Phys. Chem. C* **2008**, *112*, 18623−18627.

(3) Mathew, S.; Yella, A.; Gao, P.; Humphry-Baker, R.; Curchod, B. F.; Ashari-Astani, N.; Tavernelli, I.; Rothlisberger, U.; Nazeeruddin, M. K.; Grätzel, M. Dye-Sensitized Solar Cells with 13% Efficiency Achieved through the Molecular Engineering of Porphyrin Sensitizers. *Nat. Chem.* **2014**, *6*, 242−247.

(4) Mishra, A.; Fischer, M. K. R.; Bäuerle, P. Metal-Free Organic Dyes for Dye-Sensitized Solar Cells: From Structure: Property Relationships to Design Rules. *Angew. Chem., Int. Ed.* **2009**, *48*, 2474−2499.

(5) Liu, D.; Fessenden, R. W.; Hug, G. L.; Kamat, P. V. Dye Capped Semiconductor Nanoclusters. Role of Back Electron Transfer in the Photosensitization of SnO_2 Nanocrystallites with Cresyl Violet Aggregates. *J. Phys. Chem. B* **1997**, *101*, 2583−2590.

(6) Yella, A.; Humphry-Baker, R.; Curchod, B. F. E.; Ashari Astani, N.; Teuscher, J.; Polander, L. E.; Mathew, S.; Moser, J.-E.; Tavernelli, I.; Rothlisberger, U.; Grätzel, M.; Nazeeruddin, M. K.; Frey, J. Molecular Engineering of a Fluorene Donor for Dye-Sensitized Solar Cells. *Chem. Mater.* **2013**, *25*, 2733−2739.

(7) Kresse, G.; Furthmüller, J. Efficient Iterative Schemes for Ab Initio Total-Energy Calculations Using a Plane-Wave Basis Set. *Phys. Rev. B: Condens. Matter Mater. Phys.* **1996**, *54*, 11169−11186.

(8) Perdew, J. P.; Burke, K.; Ernzerhof, M. Generalized Gradient Approximation Made Simple. *Phys. Rev. Lett.* **1996**, *77*, 3865−3868.

(9) Lazzeri, M.; Vittadini, A.; Selloni, A. Structure and Energetics of Stoichiometric TiO_2 Anatase Surfaces. *Phys. Rev. B: Condens. Matter Mater. Phys.* **2001**, *63*, 155409.

(10) Jiao, Y.; Zhang, F.; Grätzel, M.; Meng, S. Structure−Property Relations in All-Organic Dye-Sensitized Solar Cells. *Adv. Funct. Mater.* **2013**, *23*, 424−429.

(11) Yang, H. G.; Sun, C. H.; Qiao, S. Z.; Zou, J.; Liu, G.; Smith, S. C.; Cheng, H. M.; Lu, G. Q. Anatase Tio_2 Single Crystals with a Large Percentage of Reactive Facets. *Nature* **2008**, *453*, 638−641.

(12) Meng, S.; Ren, J.; Kaxiras, E. Natural Dyes Adsorbed on TiO_2 Nanowire for Photovoltaic Applications: Enhanced Light Absorption and Ultrafast Electron Injection. *Nano Lett.* **2008**, *8*, 3266−3272.

(13) Wang, X.; Guo, L.; Xia, P. F.; Zheng, F.; Wong, M. S.; Zhu, Z. Dye-Sensitized Solar Cells Based on Organic Dyes with Naphtho[2,1-B:3,4-B[Prime or Minute]]Dithiophene as the Conjugated Linker. *J. Mater. Chem. A* **2013**, *1*, 13328−13336.

(14) Feng, Q. Y.; Jia, X. W.; Zhou, G.; Wang, Z.-S. Embedding an Electron Donor or Acceptor into Naphtho[2,1-B:3,4-B[Prime or Minute]]Dithiophene Based Organic Sensitizers for Dye-Sensitized Solar Cells. *Chem. Commun.* **2013**, *49*, 7445−7447.

(15) Zhang, J.; Li, Z. G.; Xing, H.; Zhang, W. F.; Guo, L.; Liu, Y.; Wong, M. S.; Yu, G. Naphthodithieno[3,2-B]Thiophene-Based Semiconductors: Synthesis, Characterization, and Device Performance of Field-Effect Transistors. *Org. Chem. Front.* **2014**, *1*, 333−337.

(16) Hagberg, D. P.; Marinado, T.; Karlsson, K. M.; Nonomura, K.; Qin, P.; Boschloo, G.; Brinck, T.; Hagfeldt, A.; Sun, L. C. Tuning the Homo and Lumo Energy Levels of Organic Chromophores for Dye Sensitized Solar Cells. *J. Org. Chem.* **2007**, *72*, 9550−9556.

(17) Wu, Y. Z.; Zhu, W. H. Organic Sensitizers from D-[Small Pi]-a to D-a-[Small Pi]-A: Effect of the Internal Electron-Withdrawing Units on Molecular Absorption, Energy Levels and Photovoltaic Performances. *Chem. Soc. Rev.* **2013**, *42*, 2039−2058.

(18) Wang, X. Z.; Yang, J.; Yu, H.; Li, F.; Fan, L.; Sun, W.; Liu, Y.; Koh, Z. Y.; Pan, J.; Yim, W.-L.; Yan, L.; Wang, Q. A Benzothiazole-Cyclopentadithiophene Bridged D-a-[Small Pi]-a Sensitizer with Enhanced Light Absorption for High Efficiency Dye-Sensitized Solar Cells. *Chem. Commun.* **2014**, *50*, 3965−3968.

(19) Zhu, H. B.; Li, W. Q.; Wu, Y. Z.; Liu, B.; Zhu, S. Q.; Li, X.; Ågren, H.; Zhu, W. H. Insight into Benzothiadiazole Acceptor in D−a−Π−a Configuration on Photovoltaic Performances of Dye-Sensitized Solar Cells. *ACS Sustainable Chem. Eng.* **2014**, *2*, 1026−1034.

(20) Wang, B.; Tsang, S.-W.; Zhang, W. F.; Tao, Y.; Wong, M. S. Naphthodithiophene-2,1,3-Benzothiadiazole Copolymers for Bulk Heterojunction Solar Cells. *Chem. Commun.* **2011**, *47*, 9471−9473.

(21) Yum, J.-H.; Hagberg, D. P.; Moon, S.-J.; Karlsson, K. M.; Marinado, T.; Sun, L.; Hagfeldt, A.; Nazeeruddin, M. K.; Grätzel, M. A Light-Resistant Organic Sensitizer for Solar-Cell Applications. *Angew. Chem., Int. Ed.* **2009**, *48*, 1576−1580.

(22) Sonntag, M.; Kreger, K.; Hanft, D.; Strohriegl, P.; Setayesh, S.; de Leeuw, D. Novel Star-Shaped Triphenylamine-Based Molecular Glasses and Their Use in Ofets. *Chem. Mater.* **2005**, *17*, 3031−3039.

(23) Koumura, N.; Wang, Z.-S.; Mori, S.; Miyashita, M.; Suzuki, E.; Hara, K. Alkyl-Functionalized Organic Dyes for Efficient Molecular Photovoltaics. *J. Am. Chem. Soc.* **2006**, *128*, 14256−14257.

(24) Lee, J.-K.; Lee, S.-M.; Lee, S.-B.; Kim, K.-H.; Cho, S.-E.; Jang, S.-i.; Park, S.-H.; Hwang, W.-P.; Seo, M.-H.; Kim, M.-R. Syntheses of Triphenylamine-Based Organic Dyes and Effects of Their Acceptor Groups on Photovoltaic Performances of Dye Sensitized Solar Cells. *Curr. Appl. Phys.* **2011**, *11*, S140−S146.

(25) Weng, Y.-X.; Li, L.; Liu, Y.; Wang, L.; Yang, G.-Z. Surface-Binding Forms of Carboxylic Groups on Nanoparticulate TiO_2 Surface Studied by the Interface-Sensitive Transient Triplet-State Molecular Probe. *J. Phys. Chem. B* **2003**, *107*, 4356−4363.

(26) Zhang, Q.-L.; Du, L.-C.; Weng, Y.-X.; Wang, L.; Chen, H.-Y.; Li, J.-Q. Particle-Size-Dependent Distribution of Carboxylate Adsorption Sites on TiO_2 Nanoparticle Surfaces: Insights into the Surface Modification of Nanostructured TiO_2 Electrodes. *J. Phys. Chem. B* **2004**, *108*, 15077−15083.

(27) Chen, P.; Yum, J. H.; Angelis, F. D.; Mosconi, E.; Fantacci, S.; Moon, S.-J.; Baker, R. H.; Ko, J.; Nazeeruddin, M. K.; Grätzel, M. High Open-Circuit Voltage Solid-State Dye-Sensitized Solar Cells with Organic Dye. *Nano Lett.* **2009**, *9*, 2487−2492.

(28) Bader, R. *Atoms in Molecules: A Quantum Threory*; Oxford University Press: New York, 1980.

(29) Henkelman, G.; Arnaldsson, A.; Jónsson, H. A Fast and Robust Algorithm for Bader Decomposition of Charge Density. *Comput. Mater. Sci.* **2006**, *36*, 354−360.

(30) Frisch, M. J.; Trucks, G. W.; Schlegel, H. B.; Scuseria, G. E.; Robb, M. A.; Cheeseman, J. R.; Scalmani, G.; Barone, V.; Mennucci, B.; Petersson, G. A.; Nakatsuji, H.; Caricato, M.; Li, X.; Hratchian, H. P.; Izmaylov, A. F.; Bloino, J.; Zheng, G.; Sonnenberg, J. L.; Hada, M.; Ehara, M.; Toyota, K.; Fukuda, R.; Hasegawa, J.; Ishida, M.; Nakajima, T.; Honda, Y.; Kitao, O.; Nakai, H.; Vreven, T.; Montgomery, J. A., Jr.; Peralta, J. E.; Ogliaro, F.; Bearpark, M.; Heyd, J. J.; Brothers, E.; Kudin, K. N.; Staroverov, V. N.; Kobayashi, R.; Normand, J.; Raghavachari, K.; Rendell, A.; Burant, J. C.; Iyengar, S. S.; Tomasi, J.; Cossi, M.; Rega, N.; Millam, J. M.; Klene, M.; Knox, J. E.; Cross, J. B.; Bakken, V.; Adamo, C.; Jaramillo, J.; Gomperts, R.; Stratmann, R. E.; Yazyev, O.;

DOI: 10.1021/acsami.5b07591
ACS Appl. Mater. Interfaces XXXX, XXX, XXX−XXX

Austin, A. J.; Cammi, R.; Pomelli, C.; Ochterski, J. W.; Martin, R. L.; Morokuma, K.; Zakrzewski, V. G.; Voth, G. A.; Salvador, P.; Dannenberg, J. J.; Dapprich, S.; Daniels, A. D.; Farkas, O.; Foresman, J. B.; Ortiz, J. V.; Cioslowski, J.; Fox, D. J. *Gaussian 09*, revision A.02; Gaussian, Inc.: Wallingford, CT, 2009.

(31) Francl, M. M.; Pietro, W. J.; Hehre, W. J.; Binkley, J. S.; Gordon, M. S.; DeFrees, D. J.; Pople, J. A. Self-Consistent Molecular Orbital Methods. Xxiii. A Polarization-Type Basis Set for Second-Row Elements. *J. Chem. Phys.* **1982**, *77*, 3654−3665.

(32) Hehre, W. J.; Ditchfield, R.; Pople, J. A. Self−Consistent Molecular Orbital Methods. Xii. Further Extensions of Gaussian-Type Basis Sets for Use in Molecular Orbital Studies of Organic Molecules. *J. Chem. Phys.* **1972**, *56*, 2257−2261.

(33) Jradi, F. M.; Kang, X. W.; O'Neil, D.; Pajares, G.; Getmanenko, Y. A.; Szymanski, P.; Parker, T. C.; El-Sayed, M. A.; Marder, S. R. Near-Infrared Asymmetrical Squaraine Sensitizers for Highly Efficient Dye Sensitized Solar Cells: The Effect of Π-Bridges and Anchoring Groups on Solar Cell Performance. *Chem. Mater.* **2015**, *27*, 2480−2487.

(34) van de Lagemaat, J.; Park, N. G.; Frank, A. J. Influence of Electrical Potential Distribution, Charge Transport, and Recombination on the Photopotential and Photocurrent Conversion Efficiency of Dye-Sensitized Nanocrystalline TiO_2 Solar Cells: A Study by Electrical Impedance and Optical Modulation Techniques. *J. Phys. Chem. B* **2000**, *104*, 2044−2052.

(35) Liu, J.; Yang, X. C.; Cong, J. Y.; Kloo, L.; Sun, L. C. Solvent-Free Ionic Liquid Electrolytes without Elemental Iodine for Dye-Sensitized Solar Cells. *Phys. Chem. Chem. Phys.* **2012**, *14*, 11592−11595.

DOI: 10.1021/acsami.5b07591
ACS Appl. Mater. Interfaces XXXX, XXX, XXX−XXX